IEEE Access
Multidisciplinary | Rapid Review | Open Access Journal

Received October 20, 2020, accepted October 26, 2020, date of publication October 30, 2020, date of current version November 11, 2020.

Digital Object Identifier 10.1109/ACCESS.2020.3034914

Breast Mass Classification Using eLFA Algorithm Based on CRNN Deep Learning Model

CHANG-MIN KIM[1], ROY C. PARK[2], AND ELLEN J. HONG[3]
[1]Division of Computer Information Engineering, Sangji University, Wonju 26339, South Korea
[2]Department of Information Communication Software Engineering, Sangji University, Wonju 26339, South Korea
[3]Department of Computer and Telecommunications Engineering, Yonsei University, Wonju 26493, South Korea

Corresponding author: Ellen J. Hong (jeonghee.hong@gmail.com)

This work was supported by the National Research Foundation of Korea (NRF) Grant funded by the Korea Government under Grant 2019R1F1A1060328.

ABSTRACT Breast cancer is known to be common in many developed countries. It is reported as the most common type of cancer in the US, affecting one in eight women. In Korea, thyroid cancer is the most common type of cancer, followed by breast cancer in women. Considering this, early detection and accurate diagnosis of breast cancer are crucial for reducing the associated death rate. Recently, cancer diagnosis systems using medical images have attracted significant attention. Medical imaging methods, such as computed tomography and magnetic resonance imaging, can reveal the overall shape, heterogeneity, and growth speed of carcinoma and are, thus, more commonly employed for diagnoses. Medical imaging has gained popularity since a recent study identified that it could reflect the gene phenotype of a patient. However, an aided diagnosis system based on medical images requires high-specification equipment to analyze high-resolution data. Therefore, this article proposes an edge extraction algorithm and a modified convolutional recurrent neural network (CRNN) model to accurately assess breast cancer based on medical imaging. The proposed algorithm extracts line-segment information from a breast mass image. The extracted line segments were classified into 16 types. Each type was uniquely labeled and compressed. The image compressed in this process was used as the input for the modified CRNN model. Traditional deep learning models were used to evaluate the performance of the proposed algorithm. The results show that the proposed model had the highest accuracy and lowest loss (99.75% and 0.0257, respectively).

INDEX TERMS Computer aided diagnosis system, line feature analysis, CRNN, breast cancer, deep learning.

I. INTRODUCTION

Cancer is one of the most dangerous diseases affecting humankind. It indicates a condition of the body in which the proliferation and inhibition control of cells, the smallest unit of the human body, works abnormally, destroying normal tissues. A lump of cell tissues with this characteristic is called a tumor. Cancer is classified into various types based on the location of the tumor, such as pancreatic cancer, renal cancer, and liver cancer. The danger signals of each of these are varied. The number of cancer cases has increased from 207,980 in 2010 to 229,180 in 2016, and the death rate has exhibited an increasing trend [1], [2]. Among various types of cancers, breast cancer is known to occur in numerous developed countries. Breast cancer is common in the United States with one in eight women having the disease. In Korea, breast cancer is the second most common cancer affecting women, with thyroid cancer being the most common [3]. This study focuses on breast cancer among many different types of cancers. Globally, approximately 627,000 women die of breast cancer, accounting for approximately 15% of all cancer deaths [4], [5]. At puberty, the main structure of a woman's breast is developed. In adulthood, environmental pollution and incorrect dietary habits increase the probability of breast cancer incidence. Thus, the number of breast cancer cases is expected to increase to approximately 19,300,000 by 2025 [6], [7]. It is reported that when breast cancer is diagnosed early, its prognosis is good, and the survival rate

The associate editor coordinating the review of this manuscript and approving it for publication was Yudong Zhang.

increases significantly [8]. In recent years, computer-aided diagnosis (CAD) systems have been actively researched to enable fast diagnosis and feature detection [9]–[12]. Machine learning-based methods have been proposed to expedite diagnosis and reduce the probability of misdiagnosis by medical doctors.

Schütze and Schlieter [13] found that perfect decision-making through artificial intelligence is difficult, but it effectively helps make decisions in daily human work. Mayro *et al.* [14] performed disease detection by maximizing information, such as in digital fundus images and ocular coherence tomography, using multilayer neural networks modeling the mammalian visual cortex based on a convolutional neural network (CNN). Ferrari *et al.* [15] identified complete response (CR) and nonresponders (NR) using high-resolution magnetic resonance (MR) images. After removing the unnecessary regions from the MR images using histograms and identifying the muscle region of interest (ROI), they classified patients with locally advanced rectal cancer (LARC) based on the receiver operating characteristic (ROC). Park *et al.* [16] presented a method of utilizing CNN-based organ-attention networks and statistical fusion technology for abdominal computed tomography (CT) images. Owing to the high resolution required for medical images they focus on the specific ROI, and performance is maximized by removing unnecessary areas. As the CNN-based image classification model is used, direction, contour, and spatial information are collected through a convolution operation in the ROI region and then used for prediction and diagnosis.

We propose an algorithm devised in this process. We also remove as many unnecessary areas of prediction and diagnosis as possible and reduce the dimension of the input. This process reduces the computation of the model and fixes its input dimension. In this process, we classify points, lines, and planes, which are the basic elements that make up an image, into types, and then count and reduce them. This was devised from the CNN model, an image classification neural model, in which the convolution layer extracts contours, directions, and spatial information about the input through parallel arithmetic of various kernels with the input images. When reducing the input dimension, we reduce the convolution layer used in the neural model using points, lines, and planes that constitute the image further to simplify this process. This reduces the number of parameters used in the neural model. The 160×160 input data used in this study were pre-processed and reduced to a size of 16×32. Thus, the data used are reduced to approximately one-fifth of their size. A preprocessing algorithm and a learning model are proposed to prevent the reduced data from negatively influencing the classification accuracy. This model can show accuracy similar to or higher than that of existing neural models even at lower specifications, and reduce the computational cost by reducing the amount of computation of the neural models.

The remainder of this article is organized as follows. Chapter 2 presents relevant work on breast cancer diagnosis. Chapter 3 introduces the extended line-segment feature analysis (eLFA) algorithm for pre-processing ultrasonic breast images and presents the convolutional recurrent neural network (CRNN)-based deep learning model for breast cancer diagnosis. Chapter 4 presents a comparison of the performance of the proposed algorithm and the representative image classification algorithms based on deep learning. Finally, chapter 5 concludes this study.

II. RELATED RESEARCH

A. REVIEW OF EXISTING TECHNIQUES

Machine learning and deep learning technologies are gaining popularity in cancer diagnosis research. Typical machine learning techniques include k-nearest neighbor (kNN), decision tree, artificial neural network (ANN), support vector machine (SVM), discriminant analysis, and logistic regression analysis [17]–[20]. The kNN technique classifies the new data through majority voting from the top k data that are most similar. It is highly accurate but incurs a high computation cost. The decision tree technique classifies data based on certain decision rules. It is easy to understand but yields different outcomes depending on the variable selected for branch splitting. The ANN technique classifies data to simulate the decision-making process of the human brain. Overfitting and local optimization are some of the limitations of this technique. The SVM classifies new data by predicting the hyperplane that maximizes the margin by learning the data. Compared to ANN, SVM exhibits lower overfitting and greater prediction accuracy. However, the results cannot be explained easily. The discriminant analysis determines a group of objects using the discriminant function. It is an effective technique that assumes that independent variables follow a multivariate normal distribution. Logistic regression analysis is applied when the dependent variable is categorical. It is utilized as an alternative to discriminant analysis and requires a specific assumption. No machine learning technique delivers excellent performance in every situation.

An ANN-based deep neural network delivers excellent performance in diverse fields [21]. Deep learning repeatedly executes the nonlinear conversion of input data to extract simple as well as structurally complicated features [22]–[24]. It has been proven in diverse fields that the analysis is significantly improved when these extracted features are used as inputs in a machine learning model. Particularly, the technique has actively been researched to diagnose and classify cancer to directly learn the main features of images from several ultrasonic images without additional information from experts, maximizing identification with minimal expert judgment. Among deep learning techniques, image classification and detection based on CNNs have often been applied in medical diagnosis [25], [26].

The CNN extracts features from input images and assigns weights to multiple hidden layers using convolution features. As shown in Fig. 1, a traditional CNN repeatedly applies convolutions and feature sampling to draw the final result values [27], [28]. Various forms of traditional CNNs, such

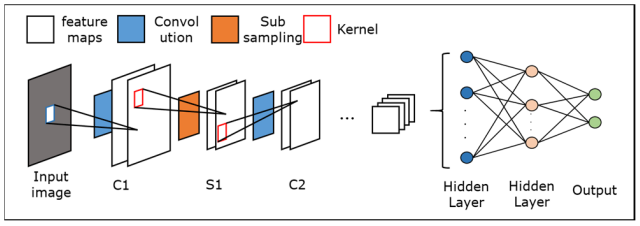

FIGURE 1. Traditional CNN Structure.

as AlexNet [29] and ZFNet [30], have been developed with a varied number of convolution layers and kernel sizes based on the number of channels. Structural performance improvement from an objective and accurate analysis of complicated medical images yields better results. However, this method has certain limitations. While image analysis using CNN-based deep learning is a model-based fast-learning and high-accuracy technique, it requires a large amount of labeled data for classification [31]. Additionally, it is difficult to maintain spatial and structural consistency in image segmentation results. This technical disadvantage results in an unclear image edge and the segmentation of unknown small regions.

The recurrent neural network (RNN) has been used to solve these technical problems. Unlike the CNN, in which the features extracted in each layer are used independently, the RNN shares these features through their connected layers such that the final output is influenced by the output of the previous layers. In the RNN, the layers serve as a type of memory [32], [33]. There is no significant difference in performance between the outcomes of the RNN and CNN-based deep learning [34]. However, RNN-based deep learning exhibits the largest difference compared to the traditional technique in terms of the extraction of the optic cup or proximal pulmonary veins [34].

This study pre-processes data to overcome the structural weakness of the CNN, which extracts edge and direction information through convolution and classifies the data in an ANN structure. The line segments of the input images are set in advance to reduce their influence on the number of convolution layers and the kernel size of the process. The proposed algorithm extracts line segment information from the images through edge detection and classifies them according to their types. Finally, it calculates the cumulative aggregate for each type of line segment to highly concentrate the images; i.e., the line segment information, drawn from the convolution layers, is set in advance and is used as the input. Thus, the number of convolution layers is reduced and setting the kernel size in the structure becomes meaningless. This study modifies a traditional CRNN model to accommodate such data learning.

B. COMPUTER-AIDED DIAGNOSIS (CAD) SYSTEMS BASED ON ARTIFICIAL INTELLIGENCE

Breast cancer is initially diagnosed through mammography. Breast ultrasound is performed when abnormal signs are found on the mammogram. Breast ultrasound imaging is used as a powerful source of data for breast cancer diagnosis as it can identify lesions that were not identified by mammography. Additionally, ultrasound images of the breast can effectively distinguish malignant tumors from benign tumors [35]. However, while ultrasound images generally show high-resolution images, the performance of the diagnosis may be reduced due to speckle noise and artifacts generated in the images. Based on these images, the ROI is identified, and feature extraction and classification are performed to identify whether the tissue is benign or malignant. This method is used as the isolation of the ROI removes the noise in the image to a great extent, and the amount of computation is reduced as unnecessary areas are removed. Diagnosis methods for identifying breast tumor characteristics based on AI can be categorized as the method using machine learning such as SVM and kNN, and the method using a CNN-based model. A mixed diagnostic method is also proposed. Yang *et al*. [36] divided the breast ultrasound image into several pieces, extracted the gray level co-occurrence matrix (GLCM) texture features as a ranklet image, and transmitted it to a SVM, showing an area under curve (AUC) of 0.918. Ding *et al*. [37] selected a breast tumor, extracted the shape of the lesion by applying a roughly segmented ROI and classified it using SVM. Ding *et al*. [38] proposed a locally weighted citation-kNN that assigns different weights to different distance vectors according to the musk benchmark dataset and the breast ultrasound image, and showed an AUC of 0.967. Tanaka *et al*. [39] selected a lesion, cut one image into three patches, and transferred them to AlexNet and VGG16 models. They classified the type of tumor based on the mean of the data calculated from each model. Their study showed an AUC of 0.909. Zhou *et al*. [40] used a 6-layer CNN model to classify malignant and benign lesions after lesion selection and shear-wave elastography (SWE) conversion through ROI in the breast ultrasound images and showed an AUC of 0.958. As shown above, studies have determined whether the tissue considered is malignant or benign based on the shape of the breast tumor. They do so based on the features of the tumors, as benign tumors have an almost smooth oval shape, and malignant tumors have an irregular surface due to necrosis and destruction of other tissues. The proposed algorithm also converts the shape of the tumor, identified using these features into line segment information, such as curves and straight lines, reducing the information on the original image data to use as input data for the model. As the input data has line segment information, a benign tumor, composed of an ellipse, will have a high aggregate value of the curve type, and a malignant will have a high aggregate value of a linear type, such as vertical, horizontal, and others. The generated data are used as inputs for the modified CRNN model to classify the tumor characteristics.

III. eLFA-CRNN MODEL TO CLASSIFY A BREAST MASS

The proposed eLFA-CRNN model analyzes the line segments of the mass in the ultrasonic breast image to assess whether

the breast mass is benign or malignant. Thus, it is called line feature analysis (LFA). The initial LFA considers the positive range of all the line segments [41]. The eLFA widens its expression, considering a negative range as well. The letter "e" in eLFA indicates the extension of the initial version of the LFA. The proposed eLFA algorithm executes the edge detection algorithm on the input image to identify the types of lines that make up the object. The data calculated using the edge detection algorithm are binary, and the line types identified are divided into 16 types through convolution with predefined filters. The classified line-type data are generated as learning data in a 16 × 32 feature map (called an eLFA map). The eLFA-CRNN model is designed and applied for the classification of breast cancer to learn the eLFA map. The following sections show the detailed processing of the eLFA algorithm.

A. THE EDGE DETECTION PROCESS OF eLFA-CRNN FOR THE EXTRACTION OF LINE SEGMENT INFORMATION

This section introduces the edge detection algorithm that converts an ultrasound breast image into line-segment information. Fig. 2 presents the breast image obtained by ultrasonography.

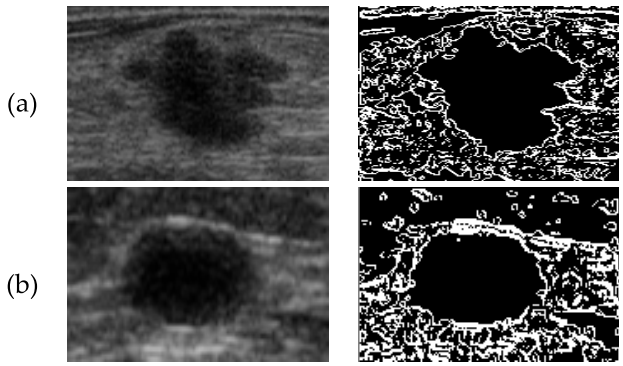

FIGURE 2. Mass of ultrasonic breast image and its edge. (a) Malignant image; (b) Benign image.

Fig. 2 illustrates a part of the real ultrasonic breast image presented by Rodrigues [42]. Fig. 2(a) shows a malignant mass, and 2(b) shows a benign mass. The edge detection results for malignant and benign lumps are presented on the right side of Fig. 2. As shown, the noise from the ultrasonic breast image is removed using edge detection. Fig.3 shows the flow of the edge detection algorithm used in the process. The algorithm detects an edge in six steps. All the areas of the ultrasonic breast image are scanned through three filters, which sets the areas as presented in (1).

$$\begin{aligned}
\mathbf{P}^{\mathrm{o}} &= [\mathrm{x}(i+r, j+s);\,(r,s) \in A], \quad (i,j) \in \mathbb{Z}^2 \\
\mathbf{P}^{\mathrm{h}} &= [\mathrm{x}(i+1+r, j+s);\,(r,s) \in A], \quad (i+1,j) \in \mathbb{Z}^2 \\
\mathbf{P}^{\mathrm{v}} &= [\mathrm{x}(i+r, j+1+s);\,(r,s) \in A], \quad (i,j+1) \in \mathbb{Z}^2 \quad (1)
\end{aligned}$$

Window A is a two-dimensional array and is set to one. A scans an area, one pixel in width and length, and moves based on $\mathbf{P}^{\mathrm{o}}$. In Equation (1), the size of A is set to 3 × 3,

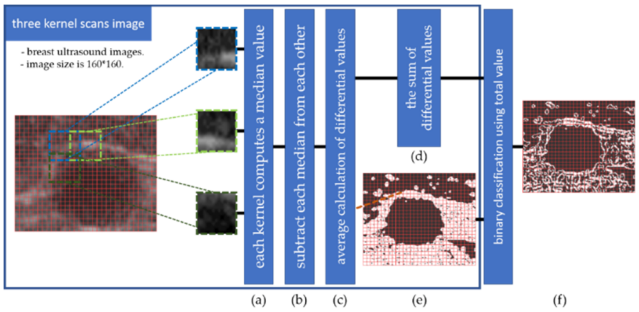

FIGURE 3. Edge detection process through ultrasonic breast image.

i and j are the values from the image size, and, r and s are the values for the size of window A. Fig. 3(a) shows the process of calculating the median values for $\mathbf{P}^{\mathrm{o}}$, $\mathbf{P}^{\mathrm{h}}$, and $\mathbf{P}^{\mathrm{v}}$, separated given by (1), and 3(b) crosses each median value calculated using 3(a) to calculate the difference.

$$\begin{aligned}
\mathbf{D}_n^{\mathrm{oh}} &= \left| \underset{\mathbf{M}_n^{\mathrm{o}}}{med}\, \mathbf{P}_n^{\mathrm{o}}(i,j) - \underset{\mathbf{M}_n^{\mathrm{h}}}{med}\, \mathbf{P}_n^{\mathrm{h}}(i,j) \right|, \\
\mathbf{D}_n^{\mathrm{ov}} &= \left| \underset{\mathbf{M}_n^{\mathrm{o}}}{med}\, \mathbf{P}_n^{\mathrm{o}}(i,j) - \underset{\mathbf{M}_n^{\mathrm{v}}}{med}\, \mathbf{P}_n^{\mathrm{v}}(i,j) \right|; (i,j) \in \mathbb{Z}^2, \quad n \in \mathbb{Z}
\end{aligned} \quad (2)$$

In Equation (2), *med* is the median. Equation (2) defines a two-dimensional median filter with a filter window $\mathbf{M}_n^{\mathrm{o}}$, $\mathbf{M}_n^{\mathrm{h}}$, $\mathbf{M}_n^{\mathrm{v}}$ on a picture $\left\{\mathbf{P}_n^{\mathrm{o}}(i,j),\,(i,j) \in \mathbb{Z}^2\right\}$, $\left\{\mathbf{P}_n^{\mathrm{h}}(i,j),\,(i,j) \in \mathbb{Z}^2\right\}$, $\left\{\mathbf{P}_n^{\mathrm{v}}(i,j),\,(i,j) \in \mathbb{Z}^2\right\}$. n is defined as $n \in$ Z. Equation (2) calculates the difference between pixel values by calculating the median value for $\mathbf{P}^{\mathrm{o}}$, $\mathbf{P}^{\mathrm{h}}$, and $\mathbf{P}^{\mathrm{v}}$ and executing the subtraction operation by crossing the calculated median value with, $\mathbf{P}^{\mathrm{o}}$, $\mathbf{P}^{\mathrm{h}}$ and $\mathbf{P}^{\mathrm{o}}$, $\mathbf{P}^{\mathrm{v}}$ (its absolute value). $\mathbf{D}^{\mathrm{oh}}$ and $\mathbf{D}^{\mathrm{ov}}$ are the values calculated through this process. Equation (2) calculates the median values of the separated pixels and finds the difference based on $\mathbf{P}^{\mathrm{o}}$. Fig. 3(c) shows the calculation of the mean value of $\mathbf{D}^{\mathrm{oh}}$ and $\mathbf{D}^{\mathrm{ov}}$. The calculated values are used in Figs. 3(d) and 3(e). In Fig. 3(d), the difference values and their means are calculated and recorded. Fig. 3(e) shows a feature map in which the difference values calculated in Fig. 3(c) are set as the status values.

Fig. 4 presents the feature map in which the mean value $((\mathbf{D}^{\mathrm{oh}}+\mathbf{D}^{\mathrm{ov}})/2)$, calculated in Fig. 3(c), is set as a status value at the edge. As shown in Fig. 4(b), the intermediate features, drawn through the three filters, are found to present the overall edge of the image. Based on the feature map, a detailed edge is detected using the mean of the difference values calculated in Fig. 3(d). The mean was used as a threshold value. Fig. 4(b) shows the detailed edge information calculated, and Fig. 4(c) presents the result of the edge detection algorithm. The LFA-based data compression was executed using edge data. Unlike a general edge detection algorithm, the proposed algorithm calculates and immediately reflects the threshold value, which is required in the detection process, so that it does not need to be set separately. While a general edge detection algorithm uses a predefined filter, the proposed

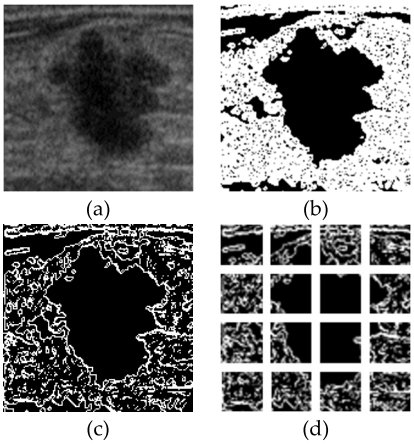

FIGURE 4. Feature map generated in edge detection process. (a) Input image; (b) Feature map consisting of mean values ($(D^{oh} + D^{ov})/2$); (c) Result data; (d) Image divided into 16 pieces.

algorithm utilizes the information drawn by scanning an input image as a filter; that is, the edge detection algorithm uses the scanned area of an input image as a filter. It can detect an edge using the threshold value calculated in the process without having to set the threshold value separately.

B. eLFA MAP GENERATION THROUGH THE EDGE INFORMATION BASED LINE SEGMENT CLASSIFICATION

In this article, an edge of the ultrasonic breast image was detected using the process described in section 3A. A series of patterns were applied to the detected edge information to classify the line segments into 16 types. Fig. 5 presents the pattern-application process.

As shown in Fig. 5(a), three steps are required to generate an eLFA map. Step 1 is to divide the edge image extracted by the process in section 3A into 16 pieces. The second step is to apply the convolution to each divided piece using a filter. The final step is to analyze the parameters of the feature map extracted from the filter, collect the same parameters, and create the final feature map. The feature map drawn in the process is called the eLFA map. It is used as an input in the learning step shown in Fig. 5(b). The traditional CRNN model was modified to enable learning of the eLFA map.

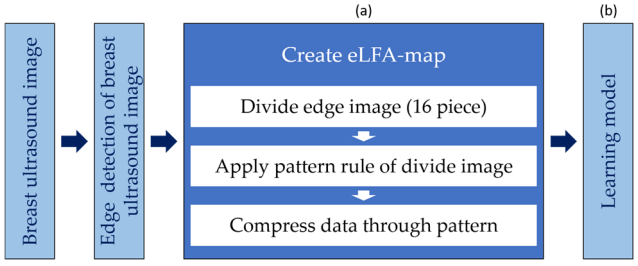

FIGURE 5. eLFA map generation process. (a) Map generation step; (b) The step for learning the generated map.

Step 1 (Divide an Edge Image): In this step, the edge image was divided into 16 pieces to present a 2D view of the eLFA map when it was generated. The 16 pieces were converted into one-dimensional arrays, each of which was stacked one layer over the other. Finally, a 2D array was generated.

Equation (3), as shown at the bottom of the page, represents the methodology of dividing an edge image into 16 pieces. In (3), $\mathbf{E}$ is the edge image, D is the size of the divided area, set to 40 in this article. $\mathbf{A}_{n,m}$ is a divided image, and M, and N are coordinate values that range from 0 to 3 in this study. In this process, after an edge image is divided, a parallel calculation can be executed in the next steps. Finally, the divided pieces are converted into one-dimensional arrays, each of which is stacked one layer over the other. Additionally, the size of the 16 pieces was reduced by max-pooling to lower operations, i.e., when an input image has a size of 160 × 160, it has sixteen 40 × 40 pieces after it is divided. Using the *max-pooling* function, the image is finally expressed as sixteen 20 × 20 pieces.

Step 2 (Apply Pattern Rule to Divided Image): The edge data processed in the previous step are divided into 16 pieces. In this step, the 16 data points are scanned using the filter $\mathbf{F}$ and then convolved. Through the operation, the visual data (line segment image) are converted into integer data.

$$\mathbf{A}_{n,m} = \begin{bmatrix} a_{0,0} & a_{0,1} & \cdots & a_{0,19} \\ a_{1,0} & a_{1,1} & & a_{1,19} \\ \vdots & & \ddots & \vdots \\ a_{19,0} & a_{1,19} & \cdots & a_{19,19} \end{bmatrix}, \quad \mathbf{F} = \begin{bmatrix} 1 & 2 \\ 4 & 8 \end{bmatrix}$$
$$\mathbf{O}_{n,m} = \mathbf{A}_{n,m} \otimes \mathbf{F}; \quad (0 \le n \le N \text{ and } 0 \le m \le M) \tag{4}$$

$$\mathbf{E} = \begin{bmatrix} a_{0,0} & a_{0,1} & \cdots & a_{0,158} & a_{0,159} \\ a_{1,0} & a_{1,1} & & a_{1,158} & a_{1,159} \\ \vdots & & \ddots & \vdots & \\ a_{159,0} & a_{159,1} & \cdots & a_{159,158} & a_{159,159} \end{bmatrix} = \begin{bmatrix} \mathbf{A}_{1,1} & \mathbf{A}_{1,2} & \mathbf{A}_{1,3} & \mathbf{A}_{1,4} \\ \mathbf{A}_{2,1} & \mathbf{A}_{2,2} & \mathbf{A}_{2,3} & \mathbf{A}_{2,4} \\ \mathbf{A}_{3,1} & \mathbf{A}_{3,2} & \mathbf{A}_{3,3} & \mathbf{A}_{3,4} \\ \mathbf{A}_{4,1} & \mathbf{A}_{4,2} & \mathbf{A}_{4,3} & \mathbf{A}_{4,4} \end{bmatrix}$$
$$\text{where,} \quad \mathbf{A}_{n,m} = \begin{bmatrix} a_{0+D*n,0+D*m} & a_{0+D*n,1+D*m} & \cdots & a_{0+D*n,38+D*m} & a_{0+D*n,39+D*m} \\ a_{1+D*n,0+D*m} & a_{1+D*n,1+D*m} & & a_{1+D*n,38+D*m} & a_{1+D*n,39+D*m} \\ \vdots & & \ddots & \vdots & \\ a_{39+D*n,0+D*m} & a_{39+D*n,1+m*D} & \cdots & a_{39+D*n,38+D*m} & a_{39+D*n,39+D*m} \end{bmatrix};$$
$$while(0 \le n \le N \text{ and } 0 \le m \le M) \tag{3}$$

TABLE 1. Type and sum of lines according to scan area.

Line Type	Filter Response Coefficient	Summing Data	Line Type	Filter Response Coefficient	Summing Data
Non-Activity	[[0,0],[0,0]]	0	Point	[[0,0],[0,1]]	8
Point	[[1,0],[0,0]]	1	Verticality	[[1,0],[0,1]]	9
Point	[[0,1],[0,0]]	2	Diagonal	[[0,1],[0,1]]	10
Horizontality	[[1,1],[0,0]]	3	Curve	[[1,1],[0,1]]	11
Point	[[0,0],[1,0]]	4	Horizontality	[[0,0],[1,1]]	12
Diagonal	[[1,0],[1,0]]	5	Curve	[[1,0],[1,1]]	13
Verticality	[[0,1],[1,0]]	6	Curve	[[0,1],[1,1]]	14
Curve	[[1,1],[1,0]]	7	Activity(Side)	[[1,1],[1,1]]	15

Equation (4) illustrates the process of applying filter **F** to all the divided pieces of the image and executing the convolution ($\otimes$). In (4), $\mathbf{A}_{n,m}$ indicates one of the pieces of the image, and n, m is the index of divided pieces. The filter **F** has 1, 2, 4, and 8 parameters. $\mathbf{O}_{n,m}$ represents the feature map drawn by the $\otimes$ of the input and the filter and has 16 data points. **A** is binarized (0: background area, 1: line segment area) by the edge detection algorithm. When the binary data and filter **F** are convolved, the result is the same as when a binary number is converted into a decimal number in engineering. During the conversion, visual data can be expressed in a decimal form. For example, if **A** has the parameters [[1, 0], [1, 1]], the internal parameters of **A** are changed into [[1, 0], [4, 8]] using **F**, and the changed results are added to generate "13." If this process is applied, the calculated value depends on the state of the internal parameters. The calculated values are equal only in the same state. The line segments are classified using the process illustrated in Table 1, according to the states of the internal parameters of **A**. "Summing Data" indicates the value calculated through the convolution of each state and the filter **F**.

Algorithm 1 Compress Data Through Pattern

Input: $[x_1, x_2, \ldots, x_n]$
def *Compress Data through Pattern*
  $Y = \text{array}(16, 32)\{0, \}$
  for x_i ***in*** $[x_1, x_2, \ldots, x_n]$ ***do***
    for w ***from*** *0* ***to*** W ***do***
      for h ***from*** *0* ***to*** H ***do***
        $Y[x_i[w, h]+16]+ = 1$ //
Output: Y

Step 3 (Compress Data Through Pattern): In the edge, images scanned with an area of 2 × 2, the dots and lines (vertical, horizontal, curved, and diagonal) were changed into a pattern of numbers based on steps 1 and 2. Using the changed values, the number of equal patterns was counted, i.e., based on the feature map drawn through convolution, the number of line segments was counted according to their types (the same number). In this case, the negative sign (-) is used to widen the expression of the data. The sum of the scanned parameters is classified into even and odd numbers. Here, the odd number is multiplied by −1. The cumulative aggregate for 1, 2, 4, 7, 11, 13, or 14 becomes a negative value. The data drawn in the process have16 one-dimensional arrays with 32 elements because the image is divided into 16 pieces, each of which is converted into a 1D array. The 16 × 32 2D array is expressed in Algorithm 1 by stacking up the 16 arrays one layer over the other. The generated 16 × 32 2D array is the eLFA map used as an input for the learning model.

C. CRNN MODEL DESIGN FOR LEARNING eLFA MAP

The eLFA map drawn from one ultrasonic breast image was used as an input for the eLFA-CRNN model. The model, designed to learn an eLFA map, comprises 8 layers, including the input and output layers, as shown in Table 2.

TABLE 2. Structure of eLFA-CRNN.

Layer No.	Layer Name
1	Input Layer (16×32)
2	Convolution (64, 16×32, std=(1, 32), pad="same", act="relu")
3	BatchNormalization
4	Reshape (2, 512)
5	Bidirectional-GRU (64)
6	Bidirectional- GRU (32)
7	Dropout (0.2)
8	Output Layer (act="sigmoid")

The traditional CRNN consists of seven convolution layers. As input data are used sequentially in each layer, the filters of the layers gradually strengthen the weak wedge and direction information and deliver it to the RNN structure. By contrast, the proposed eLFA-CRNN model pre-processes the edge information using the eLFA algorithm, such that it is meaningless to use multiple convolution layers. A highly concentrated eLFA map can negatively influence the classification as it is too small.

Thus, this study attempted to express an eLFA map in diverse ways through one convolution layer that extracts edge and direction information by controlling the filter parameters. By equating the size of a filter to that of the eLFA map, an output, similar to that of the eLFA map, can be obtained. In this study, a convolution layer was used to convert the form of expression, rather than extract edge and direction

information. Thus, layer-2 had the same filter size as the input data, as shown in Table 2, and 64 different forms of expression were generated. The feature map drawn in layer-2 prevents overfitting through layers 3 and 7. The feature map drawn in layer-3 is realigned so that its size changes to 512 and then goes to a recurrent layer. Layers 5 and 6 are recurrent layers that use a gated recurrent units (GRU) cell type.

The recurrent structure sequentially receives a variety of feature maps, and their common areas are analyzed. The difference between the previous and current inputs is classified more clearly. Layer-5 has 64 units, and layer-6 has 32. The final result is drawn in layer-7 after the recurrent layers. The learning model is used to determine whether a mass observed in an ultrasonic breast image is ''benign'' or ''malignant.'' The traditional CRNN, AlexNet, and VGG (S, M, F) models were compared with the proposed model to evaluate its performance.

IV. PERFORMANCE EVALUATION

The performance of the proposed algorithm was evaluated in the following hardware environment: Windows 10 64-bit O/S, Intel Core i7-6700 CPU, 16 GB RAM, and NVIDIA GeForce GTX 1060 6G. Keras 2.3.1, Tensorflow-gpu 2.0.0, Numpy 1.18.1, OpenCV-python 4.2, and scikit-image 0.16.2 were the software used for the evaluation. The actual ultrasonic breast image database offered by Mendeley was used as the dataset. The database had 250 datasets, 100 of which were ''benign'' data and 150 were ''malignant.'' Two tests were conducted.

The accuracies of the edge detection algorithms were measured in the first test. The proposed algorithm was compared with well-known edge detection algorithms, including the Canny, HOG, Sobel mask, and Laplacian algorithms. In the second test, the performance of the proposed eLFA-CRNN learning model was evaluated by comparing it with the CRNN, AlexNet, and VGG (S, M, F) learning models.

A. ACCURACY CHANGE OF eLFA-CRNN MODEL ACCORDING TO EDGE DETECTION ALGORITHM

This section presents the performance evaluation test for the eLFA-based edge detection algorithm by comparing it with the aforementioned well-known edge detection algorithms. Fig. 6 illustrates the results of each algorithm.

Fig. 6 presents the edge information of the ultrasonic breast image drawn using edge detection algorithms. Various parameters were applied in the tests for the conventional edge detection algorithms, and the parameter values producing the highest accuracy were set.

Fig. 7 shows the results of applying the proposed edge-detection algorithm, and four others, to the eLFA-CRNN model. Line segment information was extracted using each algorithm. In the eLFA process, the extracted line segments were classified, and a 2D array-based eLFA map was generated, which was learned by the eLFA-CRNN model designed in this study. In the tests, 80% of the database was set as learning data and 20% as test data. The classification condition was set as the ratio of the ''benign'' data to the ''malignant'' data because a simple ratio can increase the weight of one class over the other. Fig. 7(a) presents the measurement results of accuracy, and Fig. 7(b) presents the loss of each algorithm. The proposed eLFA, Canny, and Sobel-mask algorithms had the highest accuracy of 98%, and the Laplacian and HOG algorithms had accuracies of 94% and 60%, respectively. As the proposed eLFA algorithm generates a new feature map using line segments, it seems to be closely related to the edge detection results. The algorithm presented in Fig. 7(a) seems to be most similar to the edge information of the original image in Fig. 6, i.e., when an edge detection algorithm produces results that are similar to the original data, the line segment aggregate-based learning model (eLFA-CRNN model), proposed in this study, shows high accuracy. While the Sobel mask and Canny algorithms recorded a loss of 0.114 and 0.108, respectively, the eLFA algorithm recorded the lowest loss of 0.071.

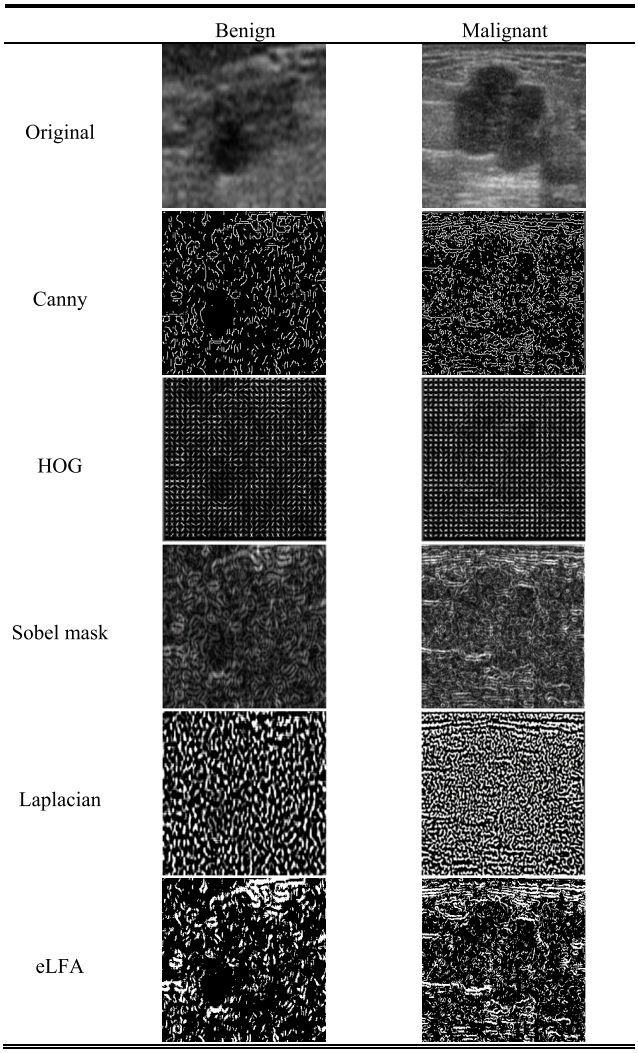

FIGURE 6. Comparison of edge information on ultrasonic breast image generated by different edge detection algorithms.

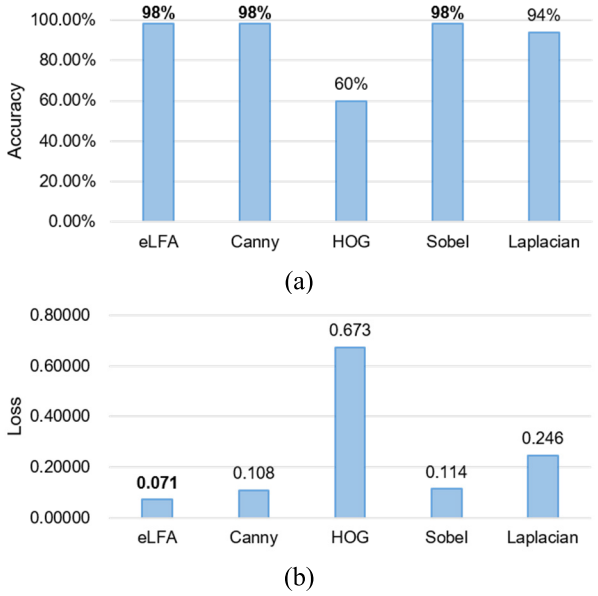

FIGURE 7. Accuracy measurement results for edge detection algorithms. (a) Accuracy; (b) Loss.

Upon testing the combinations of various parameters, the four well-known edge detection algorithms set a parameter with the highest value. As mentioned earlier, the eLFA algorithm proposed in this study does not require any parameter value to be set separately as it calculates the threshold values internally by edge detection. As a result of the accuracy measure in each edge detection algorithm, the eLFA, Canny, and Sobel-mask algorithms showed the highest accuracy of 98%. Among the algorithms, eLFA produced the lowest loss, of 0.071. Thus, the proposed eLFA algorithm shows the best performance in edge detection.

B. PERFORMANCE EVALUATION FOR eLFA-CRNN MODEL

This section describes the test conducted to evaluate the performance of the proposed eLFA-CRNN model. Additionally, the VGG-S, VGG-M, VGG-F, AlexNet, and CRNN models were used for comparison. A small amount of data (250 datasets) was used for the test and. Therefore, to increase reliability, several training-to-test data ratios were selected.

TABLE 3. Number of datasets to be used in the experiment.

Alias of experiment	Number of images(learning/test)
#1	201/ 49
#2	190/ 60
#3	170/ 80
#4	150/100

As shown in Table 3, four training and test data ratios were selected. The accuracy and loss of each model were calculated using each ratio. Fig. 8 presents the measured accuracy of the models using the selected ratios.

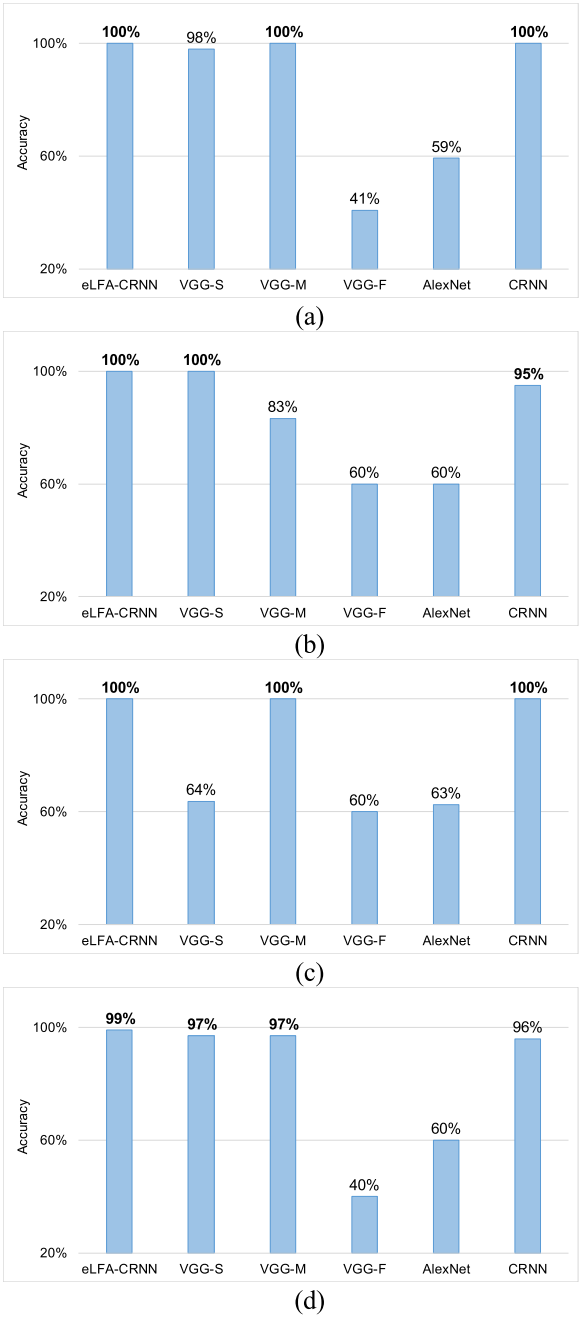

FIGURE 8. Accuracy measurement results according to the experimental environment.

In Fig. 8 (a), a training subset of 201 data points and a test subset of 49 data points were used. Consequently, the amount of training data was approximately four times larger than the amount of test data. In this case, the eLFA-CRNN, VGG-M, and CRNN models demonstrated the highest accuracy of 100%, followed by the VGG-S (98%), AlexNet (59%), and VGG-F (41%) models. The accuracy was compared by gradually reducing the training data, as shown in Figs. 8(b)–(d) to examine the learning ability of the proposed eLFA-CRNN model. Fig. 8(b) shows the accuracy of the models when the amount of training

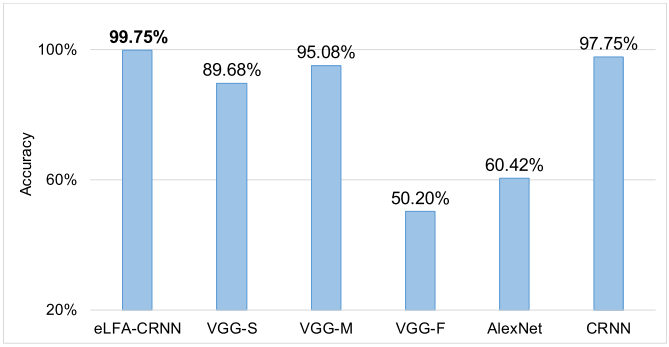

(a)

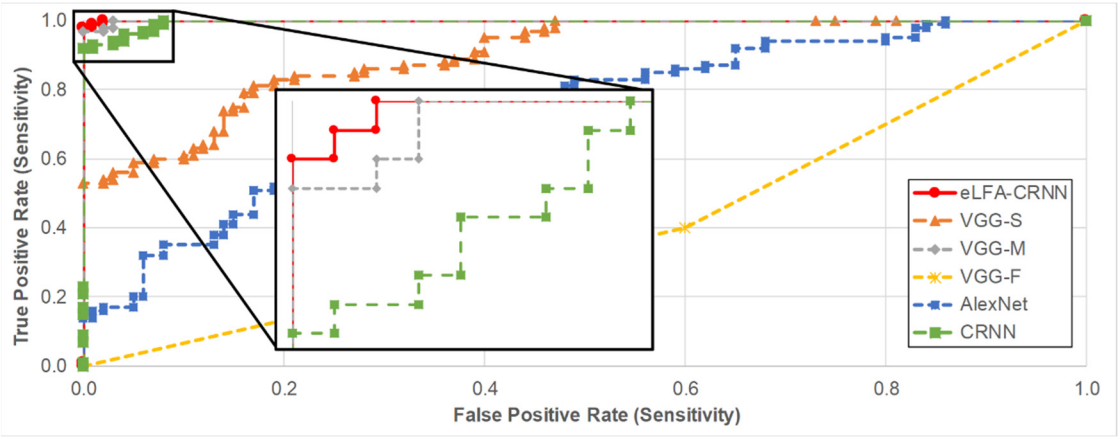

(b)

FIGURE 9. Mean results for each experiment and ROC curve.

data was about three times larger than that of the test data. The proposed eLFA-CRNN and VGG-S models also had the highest accuracy of 100% for this data split, followed by the CRNN (95%), VGG-M (83%), VGG-F (60%), and AlexNet (60%) models. Comparing the performance using data splits #1 and #2, it is observed that the performance of the VGG-S model improved. By contrast, the performance of the VGG-M and CRNN models reduced by 16.67% and 5%, respectively. Notably, the accuracy of the proposed eLFA-CRNN model for both data splits was 100%. Fig. 8(c) presents the accuracy when the training to test data ratio was 2:1.

The proposed eLFA-CRNN, VGG-M, and CRNN models produced accuracies of 100%, followed by the VGG-S (64%), and VGG-F and AlexNet (60%) models. For data splits #1 and #3, the eLFA-CRNN, VGG-M, and CRNN models showed high performance. Fig. 8(d) illustrates the accuracy in the case with 150 and 100 training and test data, respectively. In this case, the proposed eLFA-CRNN model had the highest accuracy (99%), followed by the VGG-S and VGG-M (97%), CRNN (96%), AlexNet (60%), and VGG-F (40%) models. The proposed eLFA-CRNN model produced an accuracy of 100% for data splits #1 to #3 and showed a lower performance of 99% for data split #4.

TABLE 4. Loss data measured in each experiment.

	#1	#2	#3	#4	mean
eLFA-CRNN	***0.0097***	***0.0091***	***0.0212***	***0.0621***	***0.0257***
VGG-S	0.0801	***0.0003***	0.5917	0.1230	0.1988
VGG-M	***0.0000***	0.7912	***0.0001***	0.0848	0.2190
VGG-F	0.6931	6.5572	6.4472	0.6931	3.5977
AlexNet	0.6504	0.6484	0.6641	0.6614	0.6561
CRNN	***0.0009***	0.3155	***0.0122***	0.0530	0.0956

Table 4 shows the loss data measured for each data split. As presented in Table 4 and Fig. 8, it was confirmed that the proposed eLFA-CRNN model had little performance degradation compared to the comparative model even if the data amount was changed. Additionally, with the loss of 0,0257 on average, the data for the eLFA-CRNN model was low. Thus, the proposed model supports effective classification in an environment with a small amount of training data. Fig. 9 illustrates the average accuracy and ROC curve for each test. Fig. 9(a) shows the mean accuracy calculated for each model. As shown in Fig. 9(a) and Table 4, the eLFA-CRNN model yielded the best performance with a loss data and accuracy of 0.0257 and 99.75%, respectively. Fig. 9(b) presents the

ROC curve for each test. As shown in the figure, the proposed eLFA-CRNN model demonstrates better performance than the other models evaluated.

In this article, we proposed an eLFA algorithm to reduce the dimension of the input based on the type of line segment. When identifying the type of tissue using the breast ultrasound image, the proposed algorithm reduced the computation using a more reduced layer than the existing CNN-based neural models and showed the same accuracy as the existing model. The similarity in the experimental result can be attributed to the strong feature classification performed.

Generally, if the dimension reduction technology is preceded, it degrades performance. However, when breast ultrasound images are used to identify tissue types, the shape of the lesion greatly influences on the identification of tumor type. When these trait data are processed with the proposed algorithm, the line segment for the shape is converted into aggregate data. When considering the converted data, the aggregate values for the curved and diagonal types of the oval shape increase significantly, and the other types show low aggregate values. This can be a great advantage in identifying tissue types. In objects with different shapes, the expression of aggregate values varies greatly based on their type. In these cases, strong characteristic information about the shape can be contained in the model, i.e., the segmental characteristic of the object can be emphasized when reducing the object's dimension, which can be effectively executed without losing the characteristics. Additionally, this process can reduce the computation required for the existing neural model.

TABLE 5. Comparison of the number of parameters used and the execution time of existing models and the proposed model (T-P: number of parameters used, TA-P: number of trainable parameters used, NTA-P: number of non-trainable parameters used, RT: execution time).

	T-P	TA-P	NTA-P	RT
VGG-S	56,867,266	56,867,266	0	16s
VGG-M	75,741,634	75,741,634	0	17s
VGG-F	75,539,842	75,539,842	0	21s
AlexNet	18,252,130	18,252,130	0	8s
CRNN	7,821,058	7,819,010	2048	11m 24s
eLFA	***285,698***	***285,570***	***128***	***5s***

Table 5 compares the number of parameters and execution time used by each model shown in the experiment. The proposed model shows a difference of 163.96 times that of the average value of the T-P used by the existing models. Additionally, when comparing the RT of the proposed model with the model that does not use the cyclic layer, there is no significant difference. The time is 45.6 times faster than the CRNN model using the cyclic layer. Generally, models with a cyclic layer cannot perform parallel processing, showing a relatively slower execution time than a CNN-based model. However, while the proposed model uses a cyclic layer, it can achieve faster speeds than the existing CNN-based model by reducing the number of internal calculations. If the parallel processing of the cyclic layer is performed in the future, the processing speed is expected to be faster than that of the present model. Additionally, it is expected to be applicable to embedded systems because of the simplification of the input data and the lighter weight of the learning model.

V. CONCLUSION

This study proposes an eLFA algorithm and applies it to a CRNN based learning model to classify a breast mass among masses of various other organs. The proposed eLFA algorithm was used to detect the edges of a breast mass. Unlike other algorithms, the proposed algorithm does not require a separate set of parameters and instead calculates a threshold value automatically to detect detailed line segments efficiently. The line segment information in such a process is classified into 16 types, including vertical, horizontal, curved, and diagonal. The data calculated by the edge detection algorithm are binarized and reshaped into a 2D array with elements 0 or 1 when scanned with the 2×2 area. The array then undergoes convolution using the filter [[1, 2], [4, 8]]. The convoluted area is replaced by the filter's parameter value corresponding to the parameter one position within the scanned area. The sum of the replaced areas is unique and is used to determine the type of line segment. By adding the numerical patterns cumulatively, a compressed 2D array can be generated that is used as an input for the eLFA-CRNN model, a modified CRNN model. The proposed model comprises a convolution layer and two bidirectional GRU layers. Moreover, using batch-normalization and dropout, it is possible to prevent overfitting during the learning process.

Two tests were conducted to evaluate the performance of the proposed algorithm. In the first test, the proposed eLFA algorithm was compared with the canny, HOG, Sobel mask, and Laplacian algorithms, which are generally well-known edge detection algorithms. In comparison, the proposed eLFA, canny, and Sobel algorithms delivered the highest accuracy of 98%. Furthermore, among these algorithms, the eLFA algorithm had the lowest loss of 0.0714. In the second test, the proposed eLFA-CRNN model was compared with the traditional CRNN, AlexNet, and VGG (S, M, F) models. The eLFA-CRHH model had the highest accuracy of 99.75% and the lowest loss of 0.0257. In other words, the proposed algorithm and learning model exhibited superior performance compared with other algorithms and models in terms of accuracy and data loss.

Furthermore, the proposed model exhibited a minor decline in performance and achieved effective classification in a setting with a small amount of learning data. Therefore, it is expected that the proposed model will be applicable as an effective diagnostic method in hard-to-collect data cases, as in the case of rare diseases or for diseases lacking sufficient information. In future studies, the model will be improved to detect a breast tumor rather than solely classify breast masses. Additionally, a comprehensive diagnostic system is planned using medical data that employs shape analysis, such as in cases related to skin ailments and vascular disease data.

REFERENCES

[1] Y. H. Hyeon and K. J. Moon, "Cancer care facilities nurses experience of infection control," *J. Korean Acad. Fundam. Nursing*, vol. 27, no. 1, pp. 12–28, Feb. 2020.

[2] E. H. Do and E. J. Choi, "The effect of self-efficacy and depression on sense of family coherence in cancer patients undergoing chemotherapy and primary caregivers in day care wards: Using the method actor-partner interdependence model," *Asian Oncol. Nursing*, vol. 19, no. 4, pp. 214–223, 2019.

[3] S. Y. Kwon, Y. J. Kim, and G. G. Kim, "An automatic breast mass segmentation based on deep learning on mammogram," *J. Korea Multimedia Soc.*, vol. 21, no. 12, pp. 1363–1369, 2018.

[4] S. Manohar and M. Dantuma, "Current and future trends in photoacoustic breast imaging," *Photoacoustics*, vol. 16, pp. 1–27, 2019.

[5] J. Lee and F. Vicil, "Effects of an evidence-based exercise intervention on clinical outcomes in breast cancer survivors: A randomized controlled trial," *Asian J. Kinesiol.*, vol. 22, no. 1, pp. 1–8, Jan. 2020.

[6] Y.-H. Cho, "A study of deep learning-based tumor discrimination using texture features of breast ultrasound image," *J. Korean Inst. Intell. Syst.*, vol. 30, no. 1, pp. 54–59, Feb. 2020.

[7] R. Natarajan, D. Aljaber, D. Au, C. Thai, A. Sanchez, A. Nunez, C. Resto, T. Chavez, M. M. Jankowska, T. Benmarhnia, J.-A. Yang, V. Jones, J. Tomsic, J. S. McCune, C. Sistrunk, S. Doan, M. Serrano, R. D. Cardiff, E. C. Dietze, and V. L. Seewaldt, "Environmental exposures during puberty: Window of breast cancer risk and epigenetic damage," *Int. J. Environ. Res. Public Health*, vol. 17, no. 2, pp. 1–17, 2020.

[8] J. K. Birnbaum, C. Duggan, B. O. Anderson, and R. Etzioni, "Early detection and treatment strategies for breast cancer in low-income and upper middle-income countries: A modelling study," *Lancet Glob. Health*, vol. 6, no. 8, pp. 885–893, 2018.

[9] U. R. Acharya, K. M. Meiburger, J. E. W. Koh, E. J. Ciaccio, N. Arunkumar, M. H. See, N. A. M. Taib, A. Vijayananthan, K. Rahmat, F. Fadzli, S. S. Leong, C. J. Westerhout, A. Chantre-Astaiza, and G. Ramirez-Gonzalez, "A novel algorithm for breast lesion detection using textons and local configuration pattern features with ultrasound imagery," *IEEE Access*, vol. 7, pp. 22829–22842, 2019.

[10] X. Feng *et al.*, "Accurate prediction of neoadjuvant chemotherapy pathological complete remission (pCR) for the four sub-types of breast cancer," *IEEE Access*, vol. 7, pp. 134697–134706, 2019.

[11] Y. Li, J. Wu, and Q. Wu, "Classification of breast cancer histology images using multi-size and discriminative patches based on deep learning," *IEEE Access*, vol. 7, pp. 21400–21408, 2019.

[12] L. Sun, J. Wang, Z. Hu, Y. Xu, and Z. Cui, "Multi-view convolutional neural networks for mammographic image classification," *IEEE Access*, vol. 7, pp. 126273–126282, 2019.

[13] B. Schütze and H. Schlieter, "Künstliche intelligenz," *Der Radiologe*, vol. 59, no. 12, pp. 1091–1096, 2019.

[14] E. L. Mayro, M. Wang, T. Elze, and L. R. Pasquale, "The impact of artificial intelligence in the diagnosis and management of glaucoma," *Eye*, vol. 34, no. 1, pp. 1–11, Jan. 2020.

[15] R. Ferrari, C. Mancini-Terracciano, C. Voena, M. Rengo, M. Zerunian, A. Ciardiello, S. Grasso, V. Mare, R. Paramatti, A. Russomando, R. Santacesaria, A. Satta, E. S. Camillocci, R. Faccini, and A. Laghi, "MR-based artificial intelligence model to assess response to therapy in locally advanced rectal cancer," *Eur. J. Radiol.*, vol. 118, pp. 1–9, Sep. 2019.

[16] S. Park, L. C. Chu, E. K. Fishman, A. L. Yuille, B. Vogelstein, K. W. Kinzler, K. M. Horton, R. H. Hruban, E. S. Zinreich, D. F. Fouladi, S. Shayesteh, J. Graves, and S. Kawamoto, "Annotated normal CT data of the abdomen for deep learning: Challenges and strategies for implementation," *Diagnostic Interventional Imag.*, vol. 101, no. 1, pp. 35–44, Jan. 2020.

[17] Y. Yuan and M. J. Shaw, "Induction of fuzzy decision trees," *Fuzzy Sets Syst.*, vol. 69, no. 2, pp. 125–139, Jan. 1995.

[18] G. P. Zhang, "Neural networks for classification: A survey," *IEEE Trans. Syst., Man, Cybern. C, Appl. Rev.*, vol. 30, no. 4, pp. 451–462, Nov. 2000.

[19] S. Gupta and D. Kumar, "Data mining classification techniques applied for breast cancer diagnosis and prognosis," *Indian J. Comput. Sci. Eng.*, vol. 2, no. 2, pp. 188–195, 2011.

[20] K. Kitbumrungrat, "Comparison logistic regression and discriminant analysis in classification groups for breast cancer," *Int. J. Comput. Sci. Netw. Secur.*, vol. 12, no. 5, pp. 111–115, 2012.

[21] Y. Xiao, J. Wu, Z. Lin, and X. Zhao, "A deep learning-based multi-model ensemble method for cancer prediction," *Comput. Methods Programs Biomed.*, vol. 153, pp. 1–9, Jan. 2018.

[22] B. I. Edwards, N. H. O. Khougali, and A. D. Cheok. Trends in Computer-Aided Diagnosis Using Deep 2 Learning Techniques: A Review of Recent Studies on 3 Algorithm Development 4, City University of London. 2017. [Online]. Available: https://openaccess.city.ac.uk/id/eprint/19443/

[23] S. Liu, Y. Wang, X. Yang, B. Lei, L. Liu, S. X. Li, D. Ni, and T. Wang, "Deep learning in medical ultrasound analysis: A review," *Engineering*, vol. 5, no. 2, pp. 261–275, Apr. 2019.

[24] A. S. Becker, M. Mueller, E. Stoffel, M. Marcon, S. Ghafoor, and A. Boss, "Classification of breast cancer in ultrasound imaging using a generic deep learning analysis software: A pilot study," *Brit. J. Radiol.*, vol. 91, no. 1083, pp. 1–8, 2018.

[25] M. Byra, M. Galperin, H. Ojeda-Fournier, L. Olson, M. O'Boyle, C. Comstock, and M. Andre, "Breast mass classification in sonography with transfer learning using a deep convolutional neural network and color conversion," *Med. Phys.*, vol. 46, no. 2, pp. 746–755, Feb. 2019.

[26] T. Fujioka, K. Kubota, M. Mori, Y. Kikuchi, L. Katsuta, M. Kasahara, G. Oda, T. Ishiba, T. Nakagawa, and U. Tateishi, "Distinction between benign and malignant breast masses at breast ultrasound using deep learning method with convolutional neural network," *Jpn. J. Radiol.*, vol. 37, no. 6, pp. 466–472, Jun. 2019.

[27] J. Chi, E. Walia, P. Babyn, J. Wang, G. Groot, and M. Eramian, "Thyroid nodule classification in ultrasound images by fine-tuning deep convolutional neural network," *J. Digit. Imag.*, vol. 30, no. 4, pp. 477–486, Aug. 2017.

[28] S. Y. Ko, J. H. Lee, J. H. Yoon, H. Na, E. Hong, K. Han, I. Jung, E. Kim, H. J. Moon, V. Y. Park, E. Lee, and J. Y. Kwak, "Deep convolutional neural network for the diagnosis of thyroid nodules on ultrasound," *Head Neck*, vol. 41, no. 4, pp. 885–891, Apr. 2019.

[29] A. Krizhevsky, L. Sutskever, and G. E. Hinton, "ImageNet classification with deep convolutional neural networks," in *Proc. NeurIPS*, Lake Tahoe, NV, USA, 2012, pp. 1106–1114.

[30] M. D. Zeiler and R. Fergus, "Visualizing and understanding convolutional networks," in *Proc. ECCV* Zurich, Switzerland, 2014, pp. 818–833.

[31] M. I. Razzak, S. Naz, and A. Zaib, "Deep learning for medical image processing: Overview, challenges and the future," in *Classification in BioApps*. Berlin, Germany: Springer, 2018, pp. 323–350.

[32] A. Graves and N. Jaitly, "Towards end-to-end speech recognition with recurrent neural networks," in *Proc. INML*, Beijing, China, 2014, pp. 1764–1772.

[33] A. Graves, "Supervised sequence labelling," in *Supervised Sequence Labelling with Recurrent Neural Networks*. Berlin, Germany: Springer, 2012, pp. 5–13.

[34] A. Chakravarty and J. Sivaswamy, "RACE-net: A recurrent neural network for biomedical image segmentation," *IEEE J. Biomed. Health Informat.*, vol. 23, no. 3, pp. 1151–1162, May 2019.

[35] M. Abdel-Nasser, J. Melendez, A. Moreno, O. A. Omer, and D. Puig, "Breast tumor classification in ultrasound images using texture analysis and super-resolution methods," *Eng. Appl. Artif. Intell.*, vol. 59, pp. 84–92, Mar. 2017.

[36] M.-C. Yang, W. K. Moon, Y.-C.-F. Wang, M. S. Bae, C.-S. Huang, J.-H. Chen, and R.-F. Chang, "Robust texture analysis using multi-resolution gray-scale invariant features for breast sonographic tumor diagnosis," *IEEE Trans. Med. Imag.*, vol. 32, no. 12, pp. 2262–2273, Dec. 2013.

[37] J. Ding, H. D. Cheng, J. Huang, J. Liu, and Y. Zhang, "Breast ultrasound image classification based on multiple-instance learning," *J. Digit. Imag.*, vol. 25, no. 5, pp. 620–627, Oct. 2012.

[38] J. Ding, H. D. Cheng, M. Xian, Y. Zhang, and F. Xu, "Local-weighted citation-kNN algorithm for breast ultrasound image classification," *Optik*, vol. 126, no. 24, pp. 5188–5193, Dec. 2015.

[39] H. Tanaka, S.-W. Chiu, T. Watanabe, S. Kaoku, and T. Yamaguchi, "Computer-aided diagnosis system for breast ultrasound images using deep learning," *Ultrasound Med. Biol.*, vol. 45, p. S4, 2019.

[40] Y. Zhou, J. Xu, Q. Liu, C. Li, Z. Liu, M. Wang, H. Zheng, and S. Wang, "A radiomics approach with CNN for shear-wave elastography breast tumor classification," *IEEE Trans. Biomed. Eng.*, vol. 65, no. 9, pp. 1935–1942, Sep. 2018.

[41] C. M. Kim, E. J. Hong, K. Chung, and R. C. Park, "Driver facial expression analysis using LFA-CRNN-based feature extraction for health-risk decisions," *Appl. Sci.*, vol. 10, no. 8, pp. 2956–2975, 2020.

[42] P. S. Rodrigues. (2012). *Breast Ultrasound Image, Mendeley Data*. [Online]. Available: http://dx.doi.org/10.17632/wmy84gzngw.1

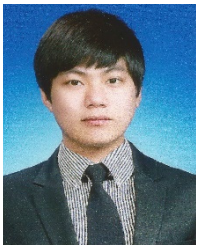

CHANG-MIN KIM received the B.S. and M.S. degrees from the Department of Computer Information Engineering, Sangji University, Wonju, South Korea, in 2014 and 2016, respectively. He is currently pursuing the Ph.D. degree with the Department of Information Communication Software Engineering, Sangji University. His research interests include computer vision, database, artificial networks, programming language, data mining, artificial intelligence, machine learning, and deep learning.

ROY C. PARK received the B.S. degree from the Department of Industrial Engineering, Sangji University, Wonju, South Korea, and the M.S. and Ph.D. degrees from the Department of Computer Information Engineering, Sangji University, in 2010 and 2015, respectively. From 2015 to 2018, he was a Professor with the Division of Computing Engineering, Dongseo University, South Korea. Since 2019, he has been a Professor with the Department of Information Communication Software Engineering, Sangji University. His research interests include WLAN systems, heterogeneous networks, ubiquitous network service, human-inspired artificial intelligent and computing, health informatics, knowledge systems, peer-to-peer, and cloud networks.

ELLEN J. HONG received the B.S. degree in electrical engineering from Pusan National University (PNU), Busan, in 2005, and the M.S. and Ph.D. degrees in electrical engineering from KAIST, Daejeon, in 2007 and 2013, respectively. She was a Postdoctoral Researcher with KAIST and PNU, from 2013 to 2016. From 2016 to 2017, she was a Professor with the Division of Computing Engineering, Dongseo University, Busan. She was a Research Engineer with the Convergence Laboratory, KT, from 2018 to 2019. Since 2019, she has been with Yonsei University, Wonju, where she is currently a Professor with the Department of Computer and Telecommunications Engineering. Her research interests include deep learning, digital twin, cyber physical systems, and evolutionary computation.